



## RESEARCH ARTICLE

10.1029/2017JD028128

## Key Points:

- A considerable proportion of gravity waves propagating energy downward are seen in the stratosphere above 15 km in winter
- The distribution of horizontal phase velocity indicates that the source of gravity waves in the lower stratosphere is the polar night jet
- Parameters of gravity waves have vertical dependencies and do not largely depend on season or their vertical group velocity direction

## Correspondence to:

Y. Minamihara,  
minamihara@eps.s.u-tokyo.ac.jp

## Citation:

Minamihara, Y., Sato, K., Tsutsumi, M., & Sato, T. (2018). Statistical characteristics of gravity waves with near-inertial frequencies in the Antarctic troposphere and lower stratosphere observed by the PANSY radar. *Journal of Geophysical Research: Atmospheres*, 123, 8993–9010. <https://doi.org/10.1029/2017JD028128>

Received 30 NOV 2017

Accepted 5 JUL 2018

Accepted article online 13 JUL 2018

Published online 3 SEP 2018

©2018. The Authors.

This is an open access article under the terms of the Creative Commons Attribution-NonCommercial-NoDerivs License, which permits use and distribution in any medium, provided the original work is properly cited, the use is non-commercial and no modifications or adaptations are made.

## Statistical Characteristics of Gravity Waves With Near-Inertial Frequencies in the Antarctic Troposphere and Lower Stratosphere Observed by the PANSY Radar

Y. Minamihara<sup>1</sup> , K. Sato<sup>1</sup> , M. Tsutsumi<sup>2</sup> , and T. Sato<sup>3</sup>

<sup>1</sup>Department of Earth and Planetary Science, The University of Tokyo, Tokyo, Japan, <sup>2</sup>National Institute of Polar Research, Tokyo, Japan, <sup>3</sup>Department of Communications and Computer Engineering, Graduate School of Informatics, Kyoto University, Kyoto, Japan

**Abstract** Gravity waves (GWs) have temporally and spatially small scales. Observations of GWs have been limited especially in the polar region due to its harsh environment. The purpose of this study is to elucidate the statistical characteristics of GWs in the Antarctic troposphere and lower stratosphere based on the continuous data over a year from 1 October 2015 to 30 September 2016 using the full system of the Program of the Antarctic Syowa MST/IS Radar (PANSY) radar at Syowa Station (69.0°S, 39.6°E). Such continuous observations over a long duration are unprecedented for high-power Mesosphere-Stratosphere-Troposphere (MST) radars at any latitude. The frequency power spectra of horizontal wind fluctuations reveal a clear isolated maximum around the inertial frequency ( $f$ ) in the lower stratosphere. A statistical analysis is performed, focusing on the GWs with near-inertial frequencies (NIGWs) that are dominant in the lower stratosphere. According to the results of hodograph analyses, there are a considerable proportion of NIGWs propagating energy downward in the upper troposphere during all seasons, as well as in the winter stratosphere above a height of 15 km, whereas NIGWs with upward group velocities are dominant in the lower troposphere and the lowermost stratosphere. These results suggest that there are NIGW sources on the ground and around the tropopause during all seasons and in the stratosphere and/or above in winter. Plausible candidates for these sources are topography, the tropospheric jet, and the polar night jet. The statistical characteristics of NIGWs, such as horizontal phase velocity, provide powerful support for our inferences of wave sources.

### 1. Introduction

Gravity waves (GWs), as well as planetary waves, play an important role in the general circulation of the middle atmosphere. GWs, most of which are generated in the troposphere, have an ability to transport momentum (mainly in the vertical direction) and deposit the momentum in the mean field through dissipation and wave-breaking processes (e.g., Alexander et al., 2010; Lindzen, 1981). In the mesosphere, momentum deposition by GWs is a major driving force of summer-to-winter pole material circulation (e.g., Plumb, 2002). This circulation not only causes mass transport but also maintains a thermal structure that differs from that expected from radiation balance only (e.g., Becker, 2012).

Many observational studies have closely focused on the characteristics of GWs in the troposphere and lower stratosphere. For the frequency spectra of GWs, some observational studies have indicated that the variances associated with GWs with near-inertial frequencies ( $f$ ) were dominant in the weak wind layer in the lower stratosphere. At midlatitudes, Sato et al. (1997) examined the characteristics of inertia-GWs using three-week continuous observations from the Middle and Upper Atmosphere Radar (MU Radar), an MST (Mesosphere-Stratosphere-Troposphere) radar located at Shigaraki, Shiga, Japan (34.9°N, 136.1°E), where the inertial period is approximately 20.9 hr. They showed the dominance of GWs with a near inertial period of ~20-hr period in the stratosphere. Nastrom and Eaton (2006) also observed dominant quasi-monochromatic oscillations with periods near the inertial frequency using hourly mean wind observations obtained from the MST radar at White Sands Missile Range, New Mexico (32.4°N, 105.9°W), and Vandenberg Air Force Base, California (34.8°N, 116.0°W). At high latitudes, Hertzog et al. (2002) indicated the enhancement of wave activity around the near-inertial frequency based on observations made using superpressure balloons launched from Kiruna, Sweden (67.9°N, 21.1°E), floating on an isopycnic surface in the lower stratosphere for several weeks as quasi-Lagrangian atmospheric tracers.

Sato et al. (1999) examined the global characteristics of GWs in the lower stratosphere by numerical simulations using a GW-permitting GCM with a horizontal resolution of T106 (i.e., a minimum resolvable horizontal wavelength of  $\sim 360$  km) and a high vertical resolution of 600 m, which did not include any GW parameterizations. The estimated horizontal wavelength of the dominant GWs with near-inertial frequencies in the lower stratosphere observed by the radar was approximately 1,200 km (Sato et al., 1997), which was large enough to be resolved in this model. The characteristics of the simulated GWs at a latitude near the MU radar site exhibited good agreement with the MU radar observations in terms of their vertical and temporal phase structures, as well as their frequency spectra. The power spectra of the horizontal wind fluctuation component had an isolated peak near  $f$  at each latitude around a height of  $z=20$  km, except for an equatorial region where  $f$  was close to 0. They also theoretically showed that the dominance of GWs with near-inertial frequencies may be explained by the poleward propagation of GWs generated by tropical convection.

For the global distribution of momentum fluxes associated with GWs, Geller et al. (2013) compared the absolute momentum fluxes from four sources of information: parameterizations of climate models, high-resolution GW permitting model simulations, satellite observations, and superpressure balloon observations. All methods exhibited large values of the absolute momentum fluxes in high latitudes of the winter hemisphere and in the subtropical region of the summer hemisphere. This comparison revealed that the GW parameterizations in most models provided excessive momentum fluxes in the polar region of the both hemispheres and also reproduce double peaks around  $50^\circ$  and  $70^\circ$ , though satellite observations and high-resolution GW-permitting models show quiet small momentum fluxes near the poles and a single peak of momentum fluxes near the latitude of the polar night jet around  $60^\circ$  in the winter hemisphere.

The deficiency of observational studies in the polar region due to its harsh environment tends to give these discrepancies in parameterized GWs at high latitudes. However, in recent years, the development of observational technology and increased scientific interest have enhanced the quantitative studies of GWs in the polar stratosphere based on observations obtained using radiosondes (Guest et al., 2000; Moffat-Griffin et al., 2011; Moffat-Griffin & Colwell, 2017; Murphy et al., 2014; Pfenninger et al., 1999; Sato & Yoshiki, 2008; Yoshiki et al., 2004; Yoshiki & Sato, 2000; Zink & Vincent, 2001), satellites (M. J. Alexander & Grimsdell, 2013; S. P. Alexander et al., 2009; Ern et al., 2011; Gong et al., 2012; Hei et al., 2008; Hindley et al., 2015; Hoffmann et al., 2013; P. Preusse et al., 2009; Wang & Alexander, 2010; Wu et al., 2006; Wu & Jiang, 2002), superpressure balloons (Hertzog et al., 2002, 2007, 2008, 2012; Rabier et al., 2010), aircraft (Fritts et al., 2016; Smith et al., 2016), and stratosphere-troposphere (ST) radars (S. Alexander & Murphy, 2015; S. P. Alexander et al., 2013; Arnault & Kirkwood, 2012; Pavelin et al., 2001; Shibuya et al., 2015; Vaughan & Worthington, 2007; Worthington & Thomas, 1997). Two campaigns of observations using superpressure balloons were carried out: the Vorcore campaign (Hertzog et al., 2007), which occurred in the spring of 2005, and the Concordiasi campaign (Rabier et al., 2010), which was performed in 2010. Both observation campaigns clarified the difference in the dynamical characteristics of GWs between those over the continent and those over the ocean: the intermittency of momentum fluxes associated with orographic GWs are larger than that associated with GWs over ocean (Jewtoukoff et al., 2015). For observations based on aircrafts, the Deep Propagating Gravity Wave Experiment (DEEPWAVE) project was also carried out over a hot spot region of GWs in New Zealand during austral winter, when the strong polar vortex edge provides a suitable environment for deep GW propagation. This project aimed to comprehensively clarify GWs rising from the troposphere to the lower thermosphere (Fritts et al., 2016). Alexander and Murphy (2015) investigated the statistical characteristic of GWs in the lower troposphere over Davis Station ( $68.6^\circ\text{S}$ ,  $78.0^\circ\text{E}$ ) based on ST radar observations obtained from September 2009 to August 2011. They showed that the lower-tropospheric ( $z=2.0\text{--}3.2$  km) GW activity reveals a maximum in winter and a minimum in summer. Their case study also indicated that the interactions between synoptic northeasterly winds and the ridgeline generate strong orographic GWs observed by the Davis radar.

At Syowa Station ( $69.0^\circ\text{S}$ ,  $39.6^\circ\text{E}$ ) in the Antarctic, Yoshiki et al. (2004) showed that the seasonal variations in wave kinetic and potential energy were dependent on height and differed from year to year. It was also noted that sporadic large values of potential energy emerged in the height region of  $z=15\text{--}25$  km when Syowa Station was near the edge of the polar vortex. Sato and Yoshiki (2008) performed three-hourly radiosonde observation campaigns over about 10 days in each month of March, June, October, and December 2002 at Syowa Station and examined the characteristics of the observed inertia GWs in the lower stratosphere.

They demonstrated that some of these GWs were likely generated from a spontaneous adjustment against a geostrophic imbalance around the polar night jet, which was located at a slightly lower latitude than Syowa Station. Yamashita et al. (2009) also examined the GW variations during the stratospheric sudden warming in the northern hemisphere in 2009 and indicated that the magnitude and occurrence of GWs correlate with the location and strength of the polar vortex that is strongly disturbed by planetary waves.

The first MST/IS (Incoherent Scatter) radar in the Antarctic, which is called the PANSY (Program of the Antarctic Syowa MST/IS Radar; Sato et al., 2014), was installed in early 2011. Initially, observations were conducted by a partial-system of the PANSY radar, which is composed of 12 out of 55 antenna groups. The full-system observation system with all 55 antenna groups was completed in March 2015, and continuous observations were successfully performed over a full year from October 2015 to September 2016. This observation is an unprecedentedly long-period campaign for MST radar observations at all latitudes. The PANSY radar is able to observe GWs in the troposphere and lower stratosphere with good accuracy and high temporal ( $\Delta t = 200$  s) and vertical ( $\Delta z = 150$  m) resolutions. Using this unique continuous observational data for one year with a high resolution enables us to analyze almost all of the entire frequency range of GWs in the troposphere and lower stratosphere ( $z = 1.5 - 22$  km).

The aim of this paper is to show the dominance of GWs with near-inertial frequencies in the lower stratosphere at Syowa Station and to elucidate the statistical characteristics of the GWs with near-inertial frequencies based on the continuous PANSY radar observations obtained over one year. We discuss the most likely sources of the GWs with near-inertial frequencies observed in each season and height region. It is worth noting that the GWs over Syowa Station are known to be not greatly different than the GWs observed over other stations in the Antarctic (Yoshiki & Sato, 2000). Thus, the characteristics of GWs over Syowa Station obtained from this study are likely to be regarded as the typical characteristics of the GWs in the coastal region of the Antarctic.

This paper is organized as follows. The descriptions of the PANSY radar data and complementary data used in this study are given in section 2. The methods used for statistical analysis, especially the extraction of GWs with near-inertial frequencies, and the details of the hodograph analysis used to estimate wave parameters are described in section 3. In section 4, the results of statistical analysis are shown and discussed. A summary and concluding remarks are given in section 5.

## 2. Data Description

### 2.1. PANSY Radar Observations

The PANSY radar was installed at Syowa Station (69.0°S, 39.6°E); it is the first Antarctic MST/IS radar (Sato et al., 2014). The PANSY radar is a monostatic pulse Doppler radar with an active phased array system consisting of 1,045 crossed-Yagi antennas and operated at a central frequency of 47 MHz. Because MST radar echoes are caused by scatter from atmospheric turbulence, MST radars are able to obtain wind measurements under any weather conditions.

A continuous full-system observation by the PANSY radar was performed over one full year from 1 October 2015 to 30 September 2016. These observations provide three-dimensional wind data, including a vertical wind component with a high accuracy of 0.1 m/s. The time resolution is approximately 60 s, and the observation time interval is approximately 200 s due to the interleaving observations from the troposphere to the lower stratosphere with those for the mesosphere. The range resolution (i.e., the vertical resolution of the vertical beam) is approximately 150 m along its beam direction for the height range of  $z = 1.5 - 17$  km, depending on the atmospheric conditions. The horizontal resolution is about 350 m at the height of 20 km and 260 m at 15 km corresponding to the beam width of 1.0°. Using data with a fine time resolution over a long observation period allows us to analyze almost all of the entire frequency range of GWs, which extends from the inertial frequency [ $f \cong 2\pi/(13h)$  at Syowa Station] to the Brunt-Väisälä frequency [ $N \cong 2\pi/(10 \text{ min})$ , a typical value for the troposphere], when the Doppler shift by the background wind is negligible. It should be noted that as the Brunt-Väisälä frequency in the stratosphere is about  $2\pi/(5 \text{ min})$ , stratospheric GWs with frequencies near the Brunt-Väisälä frequency cannot be detected by the PANSY radar. In addition, mountain waves, which may have high intrinsic frequency, are likely detected as low ground-based frequency waves (e.g., Sato, 1990). Details of the PANSY radar system have been described by Sato et al. (2014).

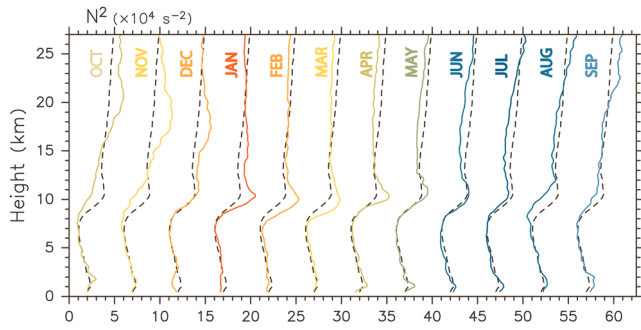


**Figure 1.** The Brunt-Väisälä frequency squared ( $N^2$ ) estimated from operational radiosonde observations during the time period of October 2015 to September 2016 (black dashed line). The colored lines correspond to the profiles of  $N^2$  for each month from October 2015 to September 2016, respectively, and each profile is shifted by  $5 \text{ s}^{-2}$ .

For the PANSY radar observations, five beams pointing to the vertical direction and to the north, east, south, and west at the same zenith angle of  $\theta = 10^\circ$  were used. Winds were estimated from the radio frequency spectra of back-scattering echo at each height by a least squares fit to a theoretically expected Gaussian function. An additional fit was conducted for the echo spectra, which are integrated for every 30 min. This method can effectively reduce the statistical noise of the echo spectra, and it allows us to estimate winds at higher altitudes to compensate for its lower temporal resolution. Note that the highest altitude where more than 30% of data are available is  $z = 17 \text{ km}$  for the original data and  $z = 22 \text{ km}$  for the 30-min integrated data. Hereafter, we refer to the data with the 30-min time resolution as the 30-min integrated data, and we refer to the data at the original time interval of 200 s as the original data. See Sato et al. (1997) for details of this wind estimation method.

Horizontal velocities are derived from the line-of-sight velocities of a symmetric beam pair  $V_{\pm\theta}$  observed by two beams with zenith angles of  $+\theta$  and  $-\theta$ , which are expressed in terms of their horizontal ( $u_{\pm\theta}$ ) and vertical wind ( $w_{\pm\theta}$ ) components as

$$V_{\pm\theta} = \pm u_{\pm\theta} \sin \theta + w_{\pm\theta} \cos \theta. \quad (1)$$

Assuming that the wind field is homogeneous between the beams at each height (i.e.,  $u_{+\theta} = u_{-\theta}$ ,  $w_{+\theta} = w_{-\theta}$ ), we can estimate the horizontal wind component  $u$  with high accuracy as follows.

$$u = \frac{V_{+\theta} - V_{-\theta}}{2 \sin \theta}. \quad (2)$$

In this study, the 30-min integrated data are mainly used to examine the characteristics of wind fluctuations mainly due to GWs.

## 2.2. Operational Radiosonde Observations

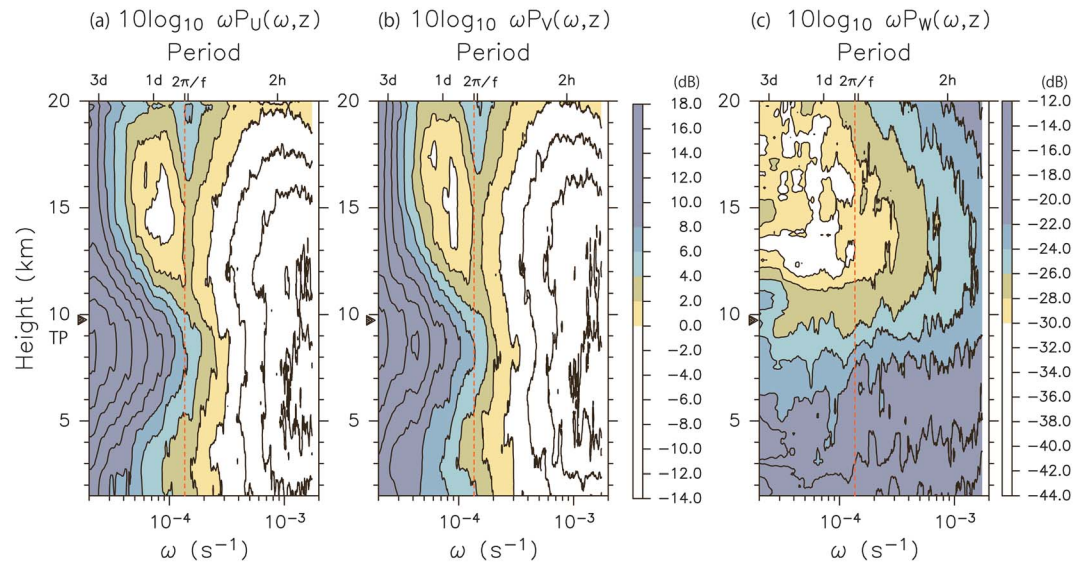
Operational radiosonde observations are made twice daily at Syowa Station at 0000UTC (0300LT) and 1200UTC (1500LT). These data are available on the Web for the height range from the surface to  $\sim 30 \text{ km}$  at vertical intervals of approximately 250 m. The temperature data obtained from the radiosondes are used to calculate the Brunt-Väisälä frequencies and tropopause height. It is also noted that the radiosondes provide horizontal wind data below  $z = 1.5 \text{ km}$ , which is the lowest observable height of the PANSY radar. Tropopause heights are determined following the definitions provided by the World Meteorological Organization (WMO).

Figure 1 shows the vertical profiles of the Brunt-Väisälä frequency squared ( $N^2$ ) averaged for one year (black broken line) and for a month (colored solid line) shifted by  $5 \times 10^{-4} \text{ s}^{-2}$  each. The seasonal variability is large in the height region of  $z = 8\text{--}12 \text{ km}$ , around the tropopause and in the vicinity of the surface. From summer to autumn, the tropopause inversion layer (e.g., Birner et al., 2002; Tomikawa et al., 2009) is observed at  $z \sim 10 \text{ km}$ . In winter, when daytime is quite short and thus ozone heating is weak, the static stability in the lower stratosphere ( $z > 9 \text{ km}$ ) is particularly weak. This weak static stability sometimes causes the apparent multiple tropopause generated by the temperature fluctuations associated with GWs (Shibuya et al., 2015). In May, the tropopause inversion layer disappears and does not appear again until December. The region with large  $N^2$  in the height of  $z > 23 \text{ km}$  in August gradually descends to a height of  $z = 15\text{--}20 \text{ km}$  in December. The vertical profiles of the mean  $N^2$  values for each month are used to estimate the horizontal wavelengths ( $\lambda_H$ ) through the dispersion relation for linear inertia-GWs (section 3.2).

## 3. Statistical Analysis Method

### 3.1. Extraction of Gravity Waves With Near-Inertial Frequencies

The frequency power spectra of horizontal and vertical wind fluctuations are calculated using the Blackman and Tukey method (Blackman & Tukey, 1959). The Blackman and Tukey method is based on



**Figure 2.** Frequency power spectra of (a) zonal ( $\omega P_U(\omega, z)$ ), (b) meridional ( $\omega P_V(\omega, z)$ ), and (c) vertical wind fluctuations ( $\omega P_W(\omega, z)$ ) in the form of energy content as a function of frequency and height. These spectra are obtained using a whole year from October 2015 to September 2016 with the 30-min integrated data from the PANSY radar. The red dashed lines correspond to the inertial frequency ( $f$ ) at Syowa Station.

the Wiener-Khinchin theorem: First, the autocorrelation function of the data series is estimated, and second, the Fourier transform of the autocorrelation, which is the power spectra of the data series, is obtained. As the autocorrelation function is a statistical function, this method can be applied to the data series including missing values. Figure 2 shows the frequency power spectra of (a) zonal ( $\omega P_U(\omega, z)$ ), (b) meridional ( $\omega P_V(\omega, z)$ ), and (c) vertical wind fluctuations ( $\omega P_W(\omega, z)$ ) in the form of their energy content form as a function of height which are calculated for the year from October 2015 to September 2016. The frequency range is from  $2\pi/(3 \text{ d})$  to  $2\pi/(1 \text{ hr})$ . For better comparison, the color scale resembles the one of the power spectra

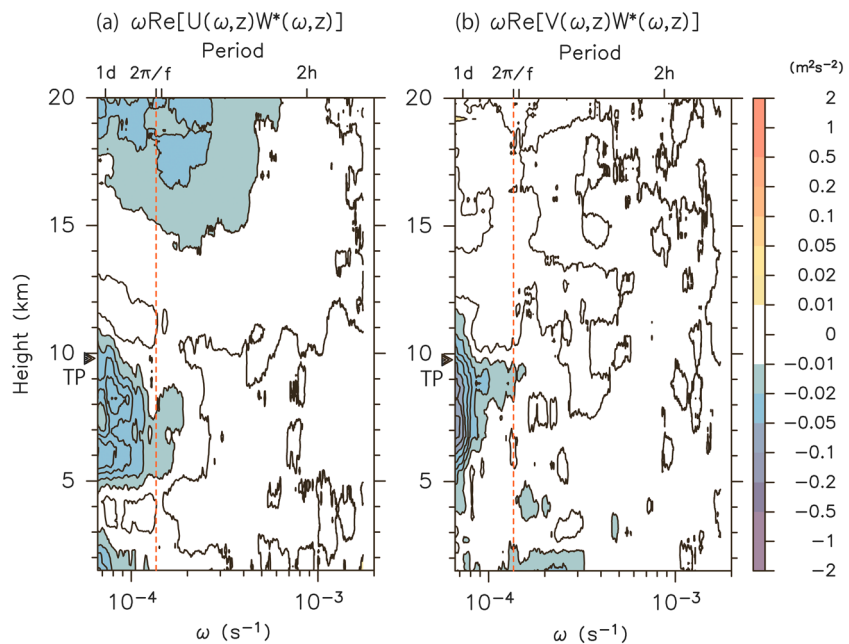


**Figure 3.** Frequency spectra of vertical flux of (a) zonal momentum ( $\omega \text{Re}[U(\omega, z)W^*(\omega, z)]$ ) and (b) meridional momentum ( $\omega \text{Re}[V(\omega, z)W^*(\omega, z)]$ ) both displayed in the flux-content form as a function of frequency and height. These spectra are obtained using the 30-min integrated data from the PANSY radar. The red dashed lines correspond to the inertial frequency ( $f$ ) at Syowa Station.

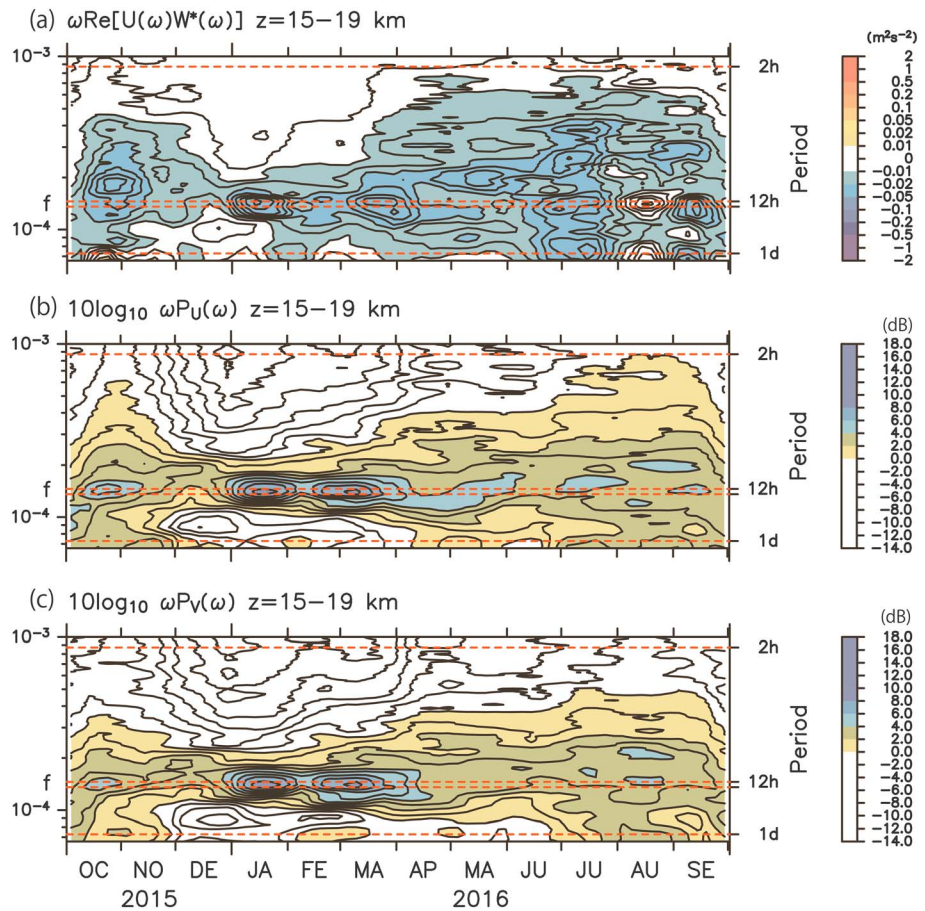


**Figure 4.** (a) Frequency spectra of the vertical fluxes of zonal momentum ( $\omega \text{Re}[U(t, \omega)W^*(t, \omega)]$ ), power spectra of (b) zonal wind ( $\omega P_u(t, \omega)$ ) and (c) meridional wind fluctuations ( $\omega P_v(t, \omega)$ ) over the height range of  $z = 15\text{--}19$  km in the flux-content form as a function of time and frequency. The red dashed lines correspond to periods of 1 day,  $2\pi/f$ , 12 and 2 hr. Spectra are estimated from the 30-min integrated data for 30 days, which are centered at every 5 days.

in Sato et al. (1999) using the MU radar observation data (Figure 3 in their paper). For  $\omega P_u(\omega, z)$  and  $\omega P_v(\omega, z)$ , an isolated maximum around the inertial frequency at Syowa Station ( $f$ ) is obvious above  $z = 11$  km. In particular, this maximum is quite remarkable in the lower stratosphere ( $z > 15$  km). In the troposphere, lower-frequency components ( $\omega < 2\pi/1$  day) are dominant, which are likely accompanied by synoptic-scale and/or medium-scale waves (e.g., Sato, 1993). For  $\omega P_w(\omega, z)$ , there is no evident peak, and higher-frequency components ( $\omega > 2\pi/12$  hr) have larger values than lower-frequency components.

The momentum flux frequency spectra ( $\omega \text{Re}[U(\omega, z)W^*(\omega, z)]$  and  $\omega \text{Re}[V(\omega, z)W^*(\omega, z)]$ ) are also estimated (see Sato et al., 2017, for details of this method) and are shown in their flux-content form in Figure 3 as a function of frequency and height. In the troposphere,  $\omega \text{Re}[U(\omega, z)W^*(\omega, z)]$  and  $\omega \text{Re}[V(\omega, z)W^*(\omega, z)]$  are negative for  $\omega < 2\pi/12$  hr. Above a height of  $z = 14$  km, negative  $\omega \text{Re}[U(\omega, z)W^*(\omega, z)]$  values are dominant in the frequency range of  $2\pi/1$  day  $< \omega < 2\pi/2$  hr, including  $f$  around which  $\omega P_u(\omega, z)$  and  $\omega P_v(\omega, z)$  clearly exhibit an isolated maximum. On the other hand, the values of  $\omega \text{Re}[V(\omega, z)W^*(\omega, z)]$  are quite small for the same frequency range.

To examine the seasonal variations in the frequency spectra around  $f$ , we obtained values of  $\omega \text{Re}[U(t, \omega)W^*(t, \omega)]$ ,  $\omega P_u(t, \omega)$ , and  $\omega P_v(t, \omega)$  in the height region of  $z = 15\text{--}19$  km using data for 30 days centered at every 5 days. Figure 4 shows  $\omega \text{Re}[U(t, \omega)W^*(t, \omega)]$ ,  $\omega P_u(t, \omega)$  and  $\omega P_v(t, \omega)$  as a function of time and frequency. For  $\omega P_u(t, \omega)$  and  $\omega P_v(t, \omega)$ , the spectral maximum around  $f$  is clearly observed during the entire time period. In particular, this maximum is sharp and has a large magnitude during the time period from January to March, whereas it is relatively broad during other months. For  $\omega \text{Re}[U(t, \omega)W^*(t, \omega)]$ , negative values are

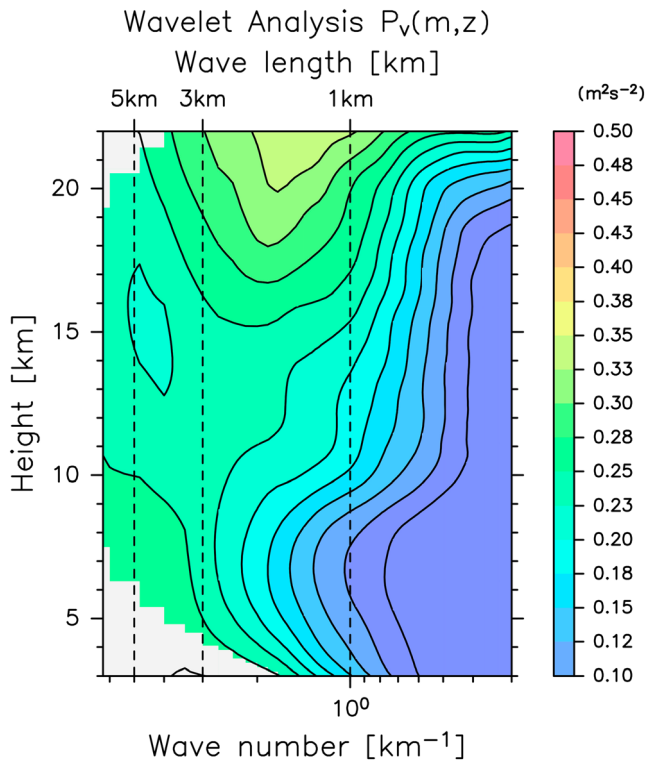


**Figure 5.** The vertical wavenumber ( $m$ ) and height section of the wavelet of meridional fluctuations ( $v'$ ) with a frequency of  $2\pi/1 \text{ day} < \omega < 2\pi/6 \text{ hr}$  averaged over one year. The insignificant region of the wavelet analysis is shown in gray.

dominant throughout the entire time period. There is a clear negative peak around  $f$  in January to March and September. A negative peak is observed at higher frequencies in October and May and broadly around  $f$  in July. The negative peak around  $f$  is absent in the middle of August. This feature may be related to an extreme event where particularly strong wind disturbances occurred in the troposphere and lower stratosphere.

To investigate the dominant vertical wavelength of the disturbances with near-inertial frequencies, we performed wavelet analysis. Figure 5 shows an average of the wavelet estimate from the vertical profile of meridional wind fluctuations with a frequency of  $2\pi/1 \text{ day} < \omega < 2\pi/6 \text{ hr}$  at each time. At vertical wavelengths of  $\lambda_z = 1\text{--}5 \text{ km}$  there is an obvious maximum in the lower stratosphere ( $z > 14 \text{ km}$ ), while there is no peak in the troposphere.

The statistical characteristics of the GWs with near-inertial frequencies ( $f$ ), which are hereafter referred to as the NIGWs, are examined by performing a hodograph analysis. The NIGW components are designated as components with frequencies of  $2\pi/(1 \text{ day}) < \omega < 2\pi/(6 \text{ hr})$  and vertical wavelengths of shorter than 5 km. These cutoff frequencies and wavelengths are determined based on the frequency spectra (Figures 2–4) and wavelet analysis in the vertical direction (Figure 5). Figure 6 shows a typical example of the time-height section of the zonal wind fluctuations associated with the NIGWs during the time period of 00UTC 18–00UTC 24 October 2015. The wave structures corresponding to the NIGWs occupy a wide height region, especially around the tropopause and the lower stratosphere. It is clear that fluctuations with upward phase velocity and downward phase velocity are frequently observed simultaneously (Figure 5a). As the hodograph analysis assumes a monochromatic wave, the NIGW component is divided into two components that propagate phase upward and downward, respectively, following Yoshiki et al. (2004), which used a two-dimensional (time and height) Fourier series expansion:

$$\begin{aligned}
 V(\omega, m) &= \sum_{i=0}^{i=N} e^{-\frac{2\pi i}{N}\omega t} \left[ \sum_{j=-\frac{M}{2}}^{j=\frac{M}{2}} V(t, z) e^{-\frac{2\pi j}{M}mz} \right] \\
 &= \sum_{i=0}^{i=N} e^{-\frac{2\pi i}{N}\omega t} \left[ \sum_{j=-\frac{M}{2}}^{j=0} V(t, z) e^{-\frac{2\pi j}{M}mz} \right] + \sum_{i=0}^{i=N} e^{-\frac{2\pi i}{N}\omega t} \left[ \sum_{j=0}^{j=\frac{M}{2}} V(t, z) e^{-\frac{2\pi j}{M}mz} \right] \quad (3)
 \end{aligned}$$

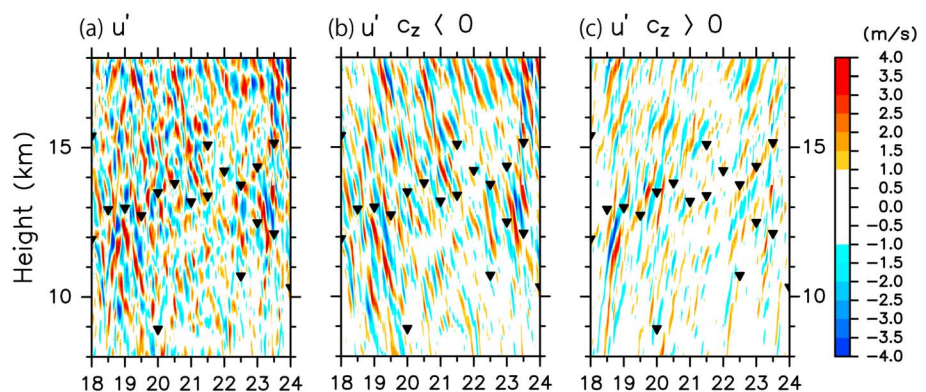


**Figure 6.** (a) The time-height section of the zonal wind of NIGWs ( $u'$ ), which have a frequency of  $2\pi/1 \text{ day} < \omega < 2\pi/6 \text{ hr}$  and a vertical wavelength of  $\lambda_z < 5 \text{ km}$  for the time period from 00UTC 18 to 00UTC 24 October 2015. The  $u'$  with downward (upward) vertical phase velocity (b) ((c)) is also shown in the time-height section for the same period. The black triangles correspond to the height of the tropopause estimated from operational radiosonde observations.

$N$  and  $M$  represent the number of data points in the time and vertical directions, respectively. The first (second) term on the rightmost side of (3) corresponds to the component with downward (upward) phase velocity. Figure 6 shows the time-height section of the NIGW components of zonal wind ( $u'$ ) with downward (Figure 6b) and upward (Figure 6c) phase speeds for the same time period as (Figure 6a). The distributions of NIGWs with downward and upward phase velocities appear to be different. The NIGWs with downward phase velocity continuously appear in the height region of  $z = 16\text{--}18$  km, while those with upward phase velocity are sporadically observed.

### 3.2. Hodograph Analysis

The hodograph analysis was performed using essentially the same method as Sato (1994), who statistically analyzed GWs at the midlatitude using MU radar observations obtained over 100 hr a month for three years. The hodograph for every 1.65-km height region (11 data points) in each vertical profile of the NIGW component of 30-min integrated data was fitted to an ellipse using the method of least squares.

The lengths of the major and minor axes of the ellipse correspond to the amplitudes of the horizontal wind components that are parallel ( $u_{\parallel}$ ) and orthogonal ( $u_{\perp}$ ) to the horizontal wave vector, respectively. The horizontal wind components  $u_{\parallel}$  and  $u_{\perp}$  are written using the zonal ( $u'$ ) and meridional ( $v'$ ) wind components:

$$\begin{aligned} u_{\parallel} &= u' \cos \theta + v' \sin \theta, \\ u_{\perp} &= -u' \sin \theta + v' \cos \theta, \end{aligned} \quad (4)$$

where  $\theta$  is the clockwise angle of the horizontal wave vector from the east. According to the polarization relation of inertia GWs, the ratio of the intrinsic frequency ( $\hat{\omega}$ ) to the inertial frequency ( $f$ ) is equal to the ratio of the amplitudes of  $u_{\parallel}$  to  $u_{\perp}$ :

$$\frac{\hat{\omega}}{f} = -i \frac{u_{\parallel}}{u_{\perp}} \quad (5)$$

When  $\hat{\omega}$  is taken to be positive without losing generality, a negative (positive)  $m$  value represents upward (downward) energy propagation (e.g., Sato, 1994). The direction of vertical energy propagation (i.e., the sign of  $m$ ) can be estimated based on the rotation of the hodograph; in the southern hemisphere, if the hodograph rotates anticlockwise (clockwise) with increasing altitude, it indicates that the GW propagates energy upward (downward).

The horizontal wavenumber ( $k$ ) was estimated using a theoretical dispersion relation for linear hydrostatic inertia-GWs. In this study, the effect of the vertical shear of the background wind was neglected, in contrast to Sato (1994), because its effect is not as large in the Antarctic troposphere and lower stratosphere as it is in the midlatitudes:

$$\begin{aligned} \hat{\omega}^2 &= f^2 + \frac{k^2 N^2}{m^2}, \\ k &= \pm \sqrt{(\hat{\omega}^2 - f^2) \cdot \frac{m^2}{N^2}}. \end{aligned} \quad (6)$$

The monthly mean  $N^2$  values for each month and height were obtained from radiosonde data (Figure 1) and using the wave parameter estimation. The sign of  $k$  was determined based on the sign of  $m$  and the covariance of  $u_{\parallel}$  and  $w$  by taking the continuity equation into account:

$$\begin{aligned} k u_{\parallel} + m w &= 0, \\ u'_{\parallel} w &= -\frac{m}{k} u'^2_{\parallel}, \end{aligned} \quad (7)$$

and hence

$$\text{sgn}(k) = -\text{sgn}(u'_{\parallel} w) \cdot \text{sgn}(m).$$

The ground-based frequency ( $\omega$ ) can be estimated based on the Doppler relation.

$$\omega = \hat{\omega} + \mathbf{U}_{\parallel} \cdot \mathbf{k} \quad (8)$$

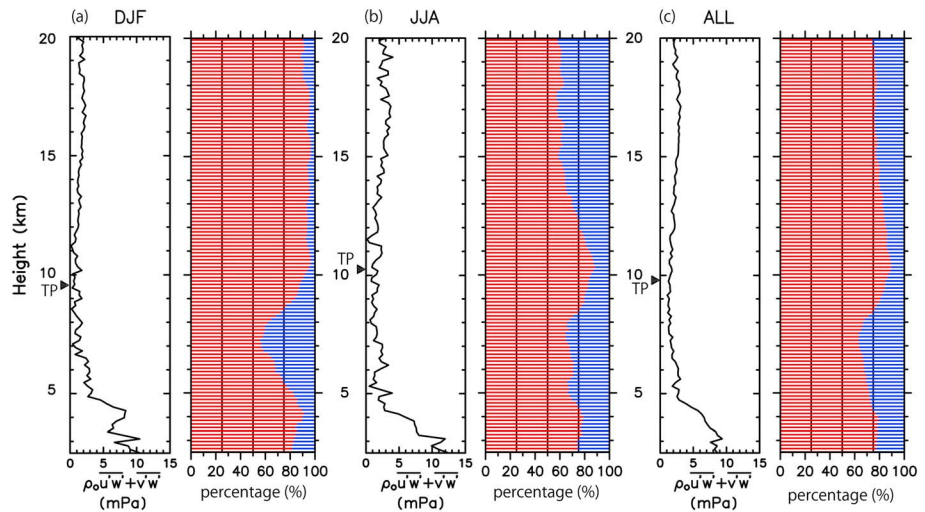


**Figure 7.** Left panels show the vertical profiles of absolute vertical momentum fluxes ( $\rho_0 \sqrt{u'w'^2 + v'w'^2}$ ) for (a) DJF, (b) JJA, and (c) one year. Right panels show the vertical profiles of the percentage of data points used for the estimation of GWs propagating energy upward (red) and downward (blue) for each time period. The black triangle on the left side of the figure indicates the average height of the tropopause over Syowa Station.

where  $\mathbf{U}_{\parallel}$  is the horizontal background wind in the direction parallel to the horizontal wave vector.  $\mathbf{U}_{\parallel}$  is obtained at the center of the height range used for fitting in the hodograph analysis by applying a low-pass filter to the 30-min integrated data with a cutoff frequency of  $2\pi/2$  day.

A linear fit with a fixed vertical wavelength ( $\lambda_z = 2\pi/m$ ) was performed to ensure that the results were stable. Among the 48 fits performed with different  $\lambda_z$  values ranging from  $0.3 \text{ km} < \lambda_z < 5.0 \text{ km}$  with an interval of 0.1 km, the wave parameters with the lowest residuals were obtained. The directions of vertical energy propagation and wave parameters such as the intrinsic frequency ( $\hat{\omega}$ ) and vertical and horizontal wavelengths ( $\lambda_z, \lambda_h$ ) were estimated only when the variance due to the elliptic wind components was larger than twice the residual, the ratio of the minor axis of the ellipse to its major axis was greater than 0.1 and smaller than 0.9, and the amplitude of the horizontal perturbation velocity in the direction of the minor axis exceeded 0.5 m/s. This method is effective for estimating the parameters of NIGWs whose amplitudes vary over both time and space. This is a merit that is absent in the Fourier transform method, which implicitly assumes that the amplitudes of waves are constant over space and/or time.

## 4. Results

### 4.1. The Profiles of the Percentages of the Vertical Group Velocities of NIGWs

Figure 7 shows the vertical profiles of vertical fluxes of the horizontal momentum due to the NIGWs ( $\rho_0 \sqrt{u'w'^2 + v'w'^2}$ ) and the percentages of the NIGWs propagating energy upward (red) and downward (blue) for December–February (DJF; Figure 7a), June–August (JJA; Figure 7b), and the whole year (Figure 7c). For  $\rho_0 \sqrt{u'w'^2 + v'w'^2}$ , the prime ( $'$ ) indicates perturbations due to NIGWs and the overbar ( $\bar{\phantom{x}}$ ) indicates the one-day temporal mean. The percentages are estimated based on the number of cases that satisfy the three criteria for hodograph analysis. The number of data points is sufficiently large to discuss the percentages of vertical group velocities: the total number of data points at each height during the year is approximately 8,000 (4,000) in the lower stratosphere (in the troposphere).

For the vertical momentum fluxes,  $\rho_0 \sqrt{u'w'^2 + v'w'^2}$  gradually increases by a factor 2 from the tropopause to the height of  $z = 17 \text{ km}$  for all profiles, while larger values are found in the lower troposphere that greatly decrease with increasing height. In DJF, the momentum fluxes are weak in the stratosphere; their values are approximately 1.5 mPa at the height of  $z = 17 \text{ km}$ , which are approximately half as large as those in JJA.

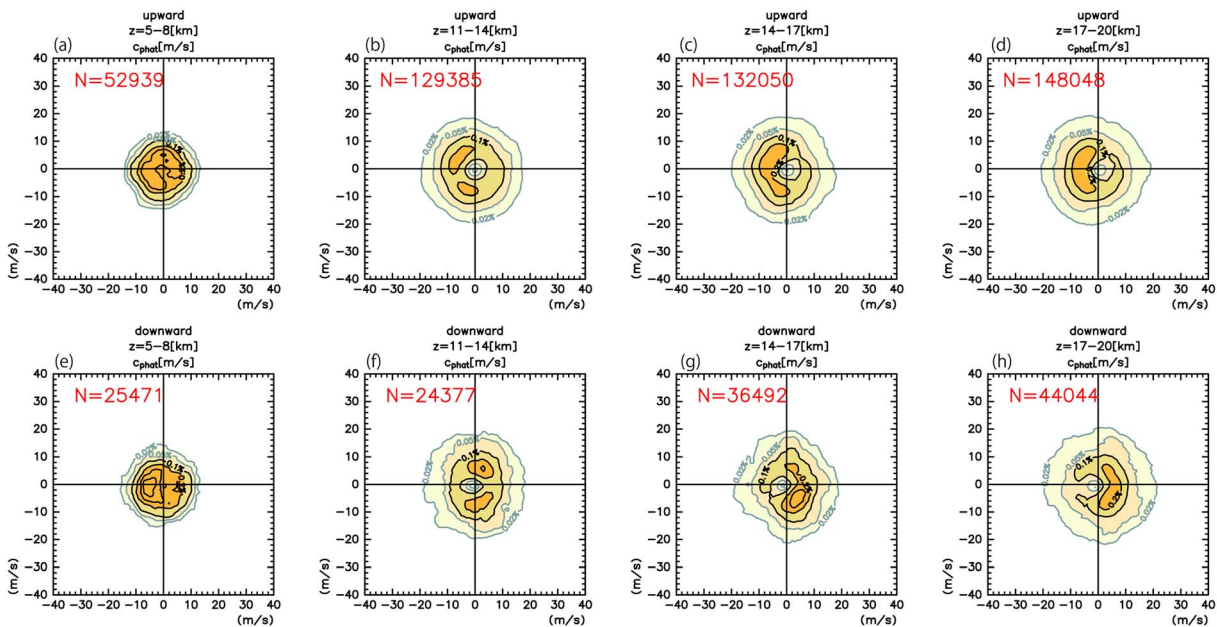


**Figure 8.** Probability density functions (PDFs) of the intrinsic horizontal phase velocities ( $\hat{c}$ ) of NIGWs with upward group velocity in the height regions of (a)  $z = 5.0 - 8.0$  km, (b)  $z = 8.0 - 11.0$  km, (c)  $z = 14.0 - 17.0$  km, and (d)  $z = 17.0 - 20.0$  km. (e–h) The results of NIGWs with downward group velocity are also shown. The contours indicate probability densities of 0.05%, 0.1%, 0.2%, and 0.5%.

In all height regions and seasons, the NIGWs propagating energy upward are dominant; in particular, the percentage of upward propagation is approximately 80% in the lower troposphere and lowermost stratosphere. On the other hand, the percentage of NIGWs with downward group velocities is relatively large (20–40%) in the upper troposphere ( $z = 6 - 7$  km) during all seasons. In addition, a significant proportion (approximately 40%) of NIGWs with downward group velocities is observed in the lower stratosphere (above  $z = 14$  km) in JJA, while in DJF, the percentage of NIGWs with downward group velocities is nearly 0.

#### 4.2. Intrinsic and Ground-Based Horizontal Phase Velocity

NIGW (Figure 8) shows the scatter diagram of the intrinsic horizontal phase velocities ( $\hat{c}$ ) of the NIGWs propagating energy upward and downward for the entire one-year period in four height regions:  $z = 5.0 - 8.0$  km,  $z = 11.0 - 14.0$  km,  $z = 14.0 - 17.0$  km, and  $z = 17.0 - 20.0$  km. The horizontal and vertical axes represent the zonal and meridional directions, respectively. The number of cases used in these calculations is shown in the upper left corner of each figure.

The directional preference in the troposphere is small compared with that in the stratosphere. In the troposphere, the probability density function (PDF) of  $\hat{c}$  is mainly distributed within a circle with a radius of  $|\hat{c}| \sim 8$  m/s. In the stratosphere, the  $\hat{c}$  of NIGWs is mainly distributed in a circle with a radius of approximately  $|\hat{c}| = 15 - 20$  m/s, but the PDF is biased toward the west (east) for NIGWs with upward (downward) group velocity.

Figure 9 is the same as Figure 8 but for the ground-based phase velocities ( $c_{\text{obs}}$ ) plotted in the same manner as  $\hat{c}$ . The ground-based phase velocity ( $c_{\text{obs}}$ ) of NIGWs is an important parameter. It is almost conserved during the vertical propagation when the background field is assumed to be steady and horizontally uniform compared with the wave period and horizontal wavelength. At the critical level where  $c_{\text{obs}} = \bar{u}(z)$ , the vertical group velocity ( $c_{gz}$ ) becomes 0 and the GWs are absorbed and deposit their momentum. For NIGWs with upward group velocity,  $c_{\text{obs}}$  is mainly distributed around  $|c_{\text{obs}}| = 0$  m/s for all height regions. The extent of the distribution becomes larger with increasing altitude. Regarding NIGWs propagating energy downward, the PDF value is large around  $|c_{\text{obs}}| = 0$  m/s in the troposphere. In the stratosphere, for NIGWs with downward group velocities, a significant proportion of ground-based phase velocities are largely biased eastward, although many of them are distributed around  $|c_{\text{obs}}| = 0$  m/s.

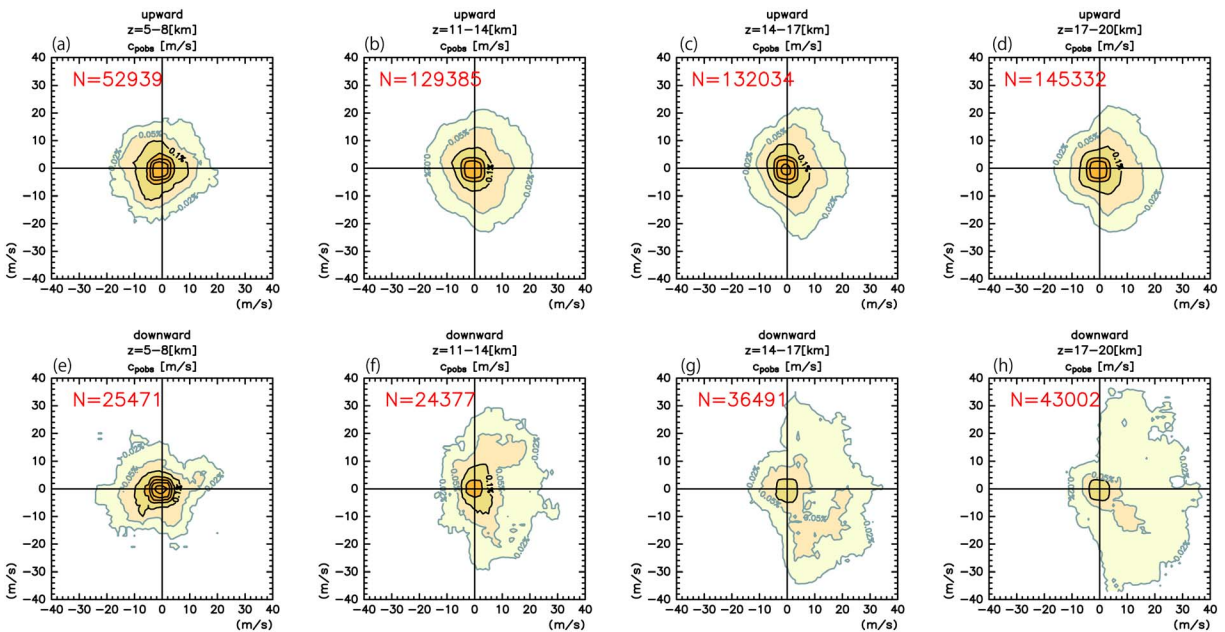


Figure 9. The same as Figure 8 but for ground-based horizontal phase velocities ( $c_{obs}$ ).

### 4.3. Vertical and Horizontal Wavelengths and Intrinsic Frequency

Statistical analyses are used to examine the vertical ( $\lambda_z$ ) and horizontal ( $\lambda_h$ ) wavelengths and intrinsic frequency ( $\hat{\omega}$ ) of NIGWs. Histograms of  $\lambda_z$  are shown separately for the NIGWs with upward and downward group velocities for each height region in Figure 10. The distribution of  $\lambda_z$  is far from the Gaussian one, and its peak is biased toward lower values. The distribution between the troposphere and the stratosphere is relatively clear.

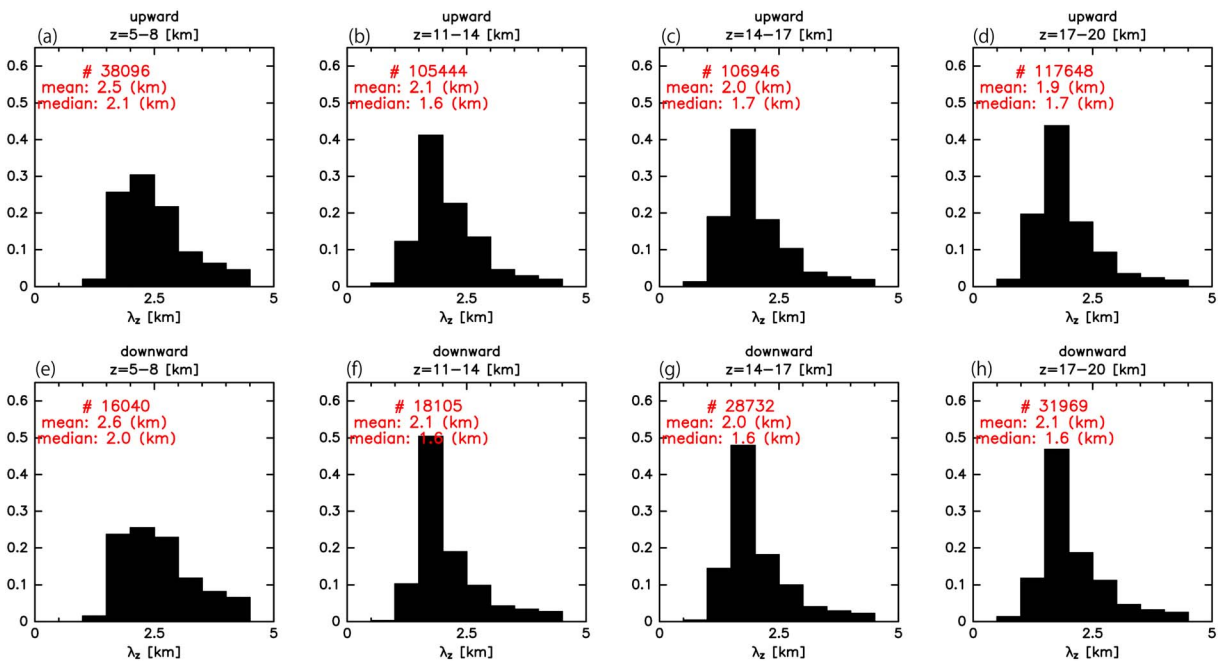


Figure 10. Histograms of vertical wavelength ( $\lambda_z$ ) values of NIGWs with upward energy propagation in the height regions of (a)  $z = 5.0 - 8.0$  km, (b)  $z = 8.0 - 11.0$  km, (c)  $z = 14.0 - 17.0$  km, and (d)  $z = 17.0 - 20.0$  km. (e-h) The results of NIGWs with downward energy propagation are also shown for the same height regions, respectively. The number of data points used for the statistical analyses, as well as their mean and median value, are shown in the upper left region of each panel.

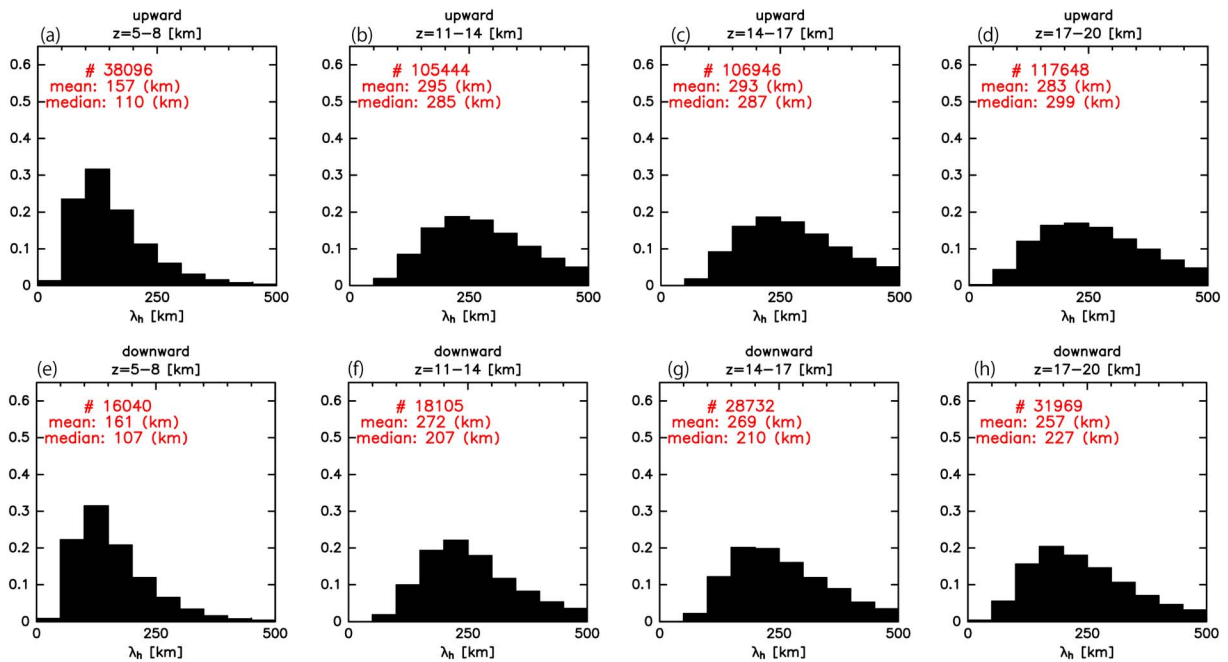


Figure 11. The same as Figure 10 but for horizontal wavelength ( $\lambda_h$ ).

There is a dominant peak in the range of  $\lambda_z = 1.5\text{--}2.0$  km in the lower stratosphere, while a main peak exists in the range of  $\lambda_z = 2.0\text{--}2.5$  km in the troposphere. There are no clear differences in the distribution or mean and median values between the three height regions in the stratosphere or between the upward and downward directions of the vertical group velocity. The mean value is approximately 2.0 km and the median value is 1.6–1.7 km in all histograms.

Figure 11 shows the histograms for  $\lambda_h$ . Similar to  $\lambda_z$ , the distributions of  $\lambda_h$  is slightly different between the troposphere and the stratosphere: In the troposphere, a sharp peak exists in the range of  $\lambda_h = 100\text{--}150$  km, whereas in the stratosphere, a broad maximum exists in the range of  $\lambda_h = 150\text{--}200$  km. In the stratosphere, NIGWs with upward group velocity have relatively large mean and median values compared to those with downward group velocity. For NIGWs with downward group velocity, the peak is biased toward smaller values relative to those with upward group velocity.

Figure 12 shows the histogram of the ratios of the intrinsic frequency to the inertial frequency ( $f/\hat{\omega}$ ). The distributions of  $f/\hat{\omega}$  are different between the troposphere and the stratosphere. In the troposphere, a peak exists in the range of  $f/\hat{\omega} = 0.5\text{--}0.7$  and the distributions are close to being Gaussian, whereas in the stratosphere, a dominant peak is observed in the range of  $0.7\text{--}0.8$ , whereas the peak in the troposphere is widely seen in the range of  $0.5\text{--}0.7$ . In the stratosphere, only the histogram for NIGWs with downward group velocity in the height region of  $z = 17.0\text{--}20.0$  km has a gentle peak around  $0.6\text{--}0.7$ , even though others have a dominant peak around  $0.7\text{--}0.8$ .

Figure 13 summarizes the mean value ((a)  $\lambda_z$ , (b)  $\lambda_h$ , and (c)  $f/\hat{\omega}$ ) as a function of height for the NIGWs propagating energy upward (thick) and downward (thin) in JJA (red), DJF (blue), and during one year (black), respectively. The mean values estimated from fewer than 1,000 data points are not shown. Each parameter varies substantially between the troposphere and stratosphere, but they do not greatly depend on the season (color) or the direction (thickness) of vertical energy propagation. Although the mean value of  $\lambda_z$  does not largely depend on the season, the NIGWs in DJF have a longer  $\lambda_h$  and  $f/\hat{\omega}$  values that are closer to 1 than those in JJA, especially in the height region above  $z = 15.0$  km. The Brunt-Väisälä frequency ( $N$ ) largely affects the estimation of horizontal wavelength ( $\lambda_h$ ) via the dispersion relation. Thus, the uncertainty in the mean value of  $\lambda_h$  may be large around the tropopause where  $N$  is discontinuous, because the monthly mean  $N$  is used for the estimation.

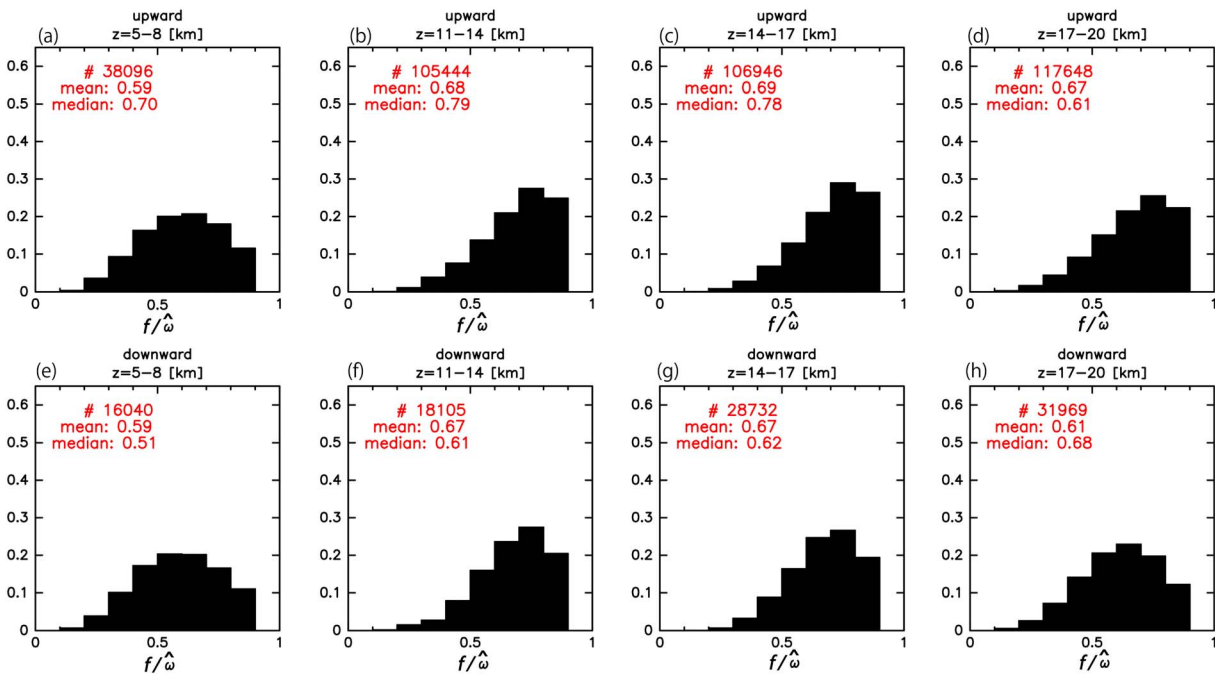


Figure 12. The same as Figure 10 but for the ratio between the intrinsic frequency and the inertial frequency ( $f/\hat{\omega}$ ).

#### 4.4. Discussion

A strikingly large percentage of NIGWs with downward group velocity can be seen in the upper troposphere during all seasons and in the lower stratosphere above  $z=15$  km in JJA, whereas the NIGWs with upward group velocity are dominant in all height regions, especially those near the surface and in the lowermost stratosphere (Figure 7). This result suggests that the sources of NIGWs observed at Syowa Station are likely

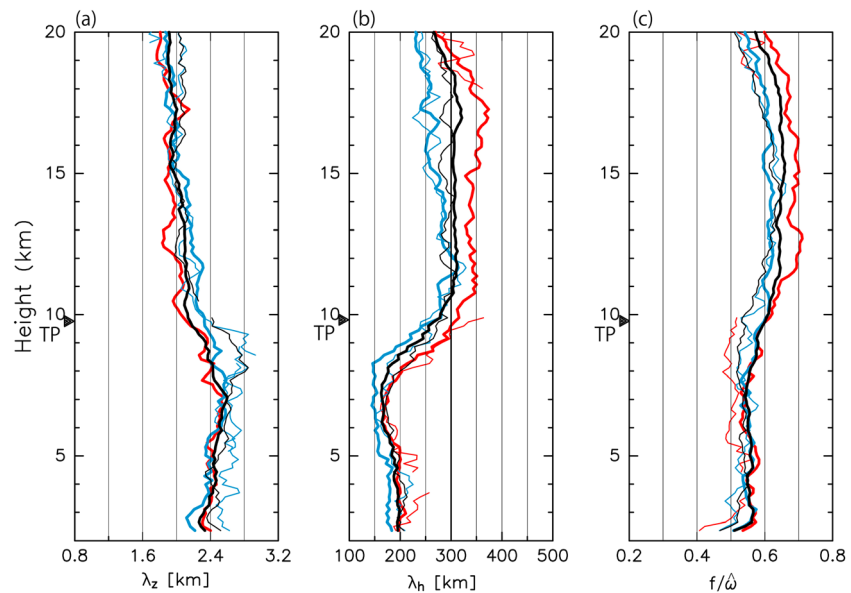


Figure 13. The vertical profiles of (a) vertical wavelength ( $\lambda_z$ ), (b) horizontal wavelength ( $\lambda_h$ ), and (c) the ratio between the intrinsic frequency and the inertial frequency ( $f/\hat{\omega}$ ). The thick (thin) lines indicate the mean values of NIGWs with upward (downward) energy propagating over one year (black), in JJA (blue) and in DJF (red). The mean values estimated from small numbers (<1,000) of data points are not shown. The black triangle on the left side of the figure indicates the yearly average height of the tropopause over Syowa Station.

present near the surface, around the tropopause, and in the upper stratosphere or above. In addition, the statistical characteristics of the NIGW parameters, such as  $\lambda_z$ ,  $\lambda_h$ , and  $f/\widehat{\omega}$ , vary substantially between the troposphere and the stratosphere (Figures 10–13). This may be due to the following plausible theoretical explanation. First, for a range of  $m$  analyzed in the stratosphere, larger  $N^2$  values tend to give longer  $\lambda_h$  values than in the troposphere so that the dispersion relation is satisfied. Second, different wave parameters may be attributed to differences in the dominant wave sources in the troposphere and lower stratosphere.

There is further evidence that supports the possibility that NIGWs are generated by the various sources, as mentioned above. The NIGWs with upward group velocities have ground-based phase velocities ( $\mathbf{c}_{\text{obs}}$ ) that are approximately close to 0 (Figure 9), which is consistent with the characteristics of topographically forced GWs near the surface. On the other hand, there is a significant proportion of GWs with downward group velocities in the winter that have largely eastward ground-based phase velocities ( $\mathbf{c}_{\text{obs}}$ ). This strongly supports the possibility that the NIGWs originate from sources moving eastward. A likely candidate for such a source is the polar night jet blowing eastward that appears in the winter stratosphere. Furthermore, the histogram of the  $f/\widehat{\omega}$  values of NIGWs with downward group velocities in the height region of  $z=17\text{--}20$  km is different than the other histograms of NIGWs with upward group velocities, which may also suggest the existence of different sources. Another possible process is a partial reflection of NIGWs at the tropopause where  $N^2$  increases discontinuously in the vertical (Figure 1).

Minamiyama et al. (2016) showed, based on three-year continuous PANSY radar observations, that the most likely source of NIGWs in the lower troposphere ( $z=1.5\text{--}4.0$  km) was topography. This conclusion was supported by the fact that the vertical wind disturbances near the surface are active when the horizontal wind near the surface is strong and the fact that the height of  $\bar{u} = 0$  m/s corresponds to the top of the active vertical wind disturbances. Their suggestion that the most plausible source of GWs is the topography around Syowa Station is consistent with the results shown in this study, that is, the dominance of NIGWs with upward group velocities in the lower troposphere and the distribution of  $\mathbf{c}_{\text{obs}}$  values around 0 m/s for NIGWs with upward group velocities in the troposphere.

The statistical results demonstrating that the percentage of NIGWs with upward (downward) group velocities in the lowermost stratosphere (upper troposphere) is large during all seasons are consistent with the results of Hirota and Niki (1986), which were based on MU radar observations at midlatitudes. They showed that inertia GWs propagate energy downward in the upper troposphere and upward in the lowermost stratosphere and suggested that the strong tropopause westerly jet is the most likely source of the GWs. The upward and downward GW emission is enhanced downstream of the jet streak, as was shown from radiosonde (Plougonven et al., 2003) and radar observations (Pavelin et al., 2001; Thomas et al., 1999) and model-simulations (Zülicke & Peters, 2006).

The large percentage of NIGWs propagating energy downward in winter is consistent with the results of the previous observational study at Syowa Station performed by Sato and Yoshiki (2008), which were based on 3-hourly radiosonde observations. They showed that GWs propagating energy downward existed in the Antarctic lower stratosphere when the polar night jet was located at a slightly lower latitude than Syowa Station with a large local Rossby number. They also suggested that the observed inertia GWs in the winter lower stratosphere were likely generated by a spontaneous adjustment around the unbalanced polar night jet.

Finally, we compare the parameters of the GWs observed by MST radars at midlatitudes. According to Sato (1994), who examined the statistics of the parameters of inertia GWs based on MU radar observations, the mean value of  $\lambda_z$  is 2.0 km in winter and 1.6 km in summer and that of  $\lambda_h$  is approximately 300 km during all seasons in the height region of  $z=16\text{--}22$  km. These mean values are not substantially different than the results obtained using the PANSY radar observations, that is,  $\lambda_z=1.9\text{--}2.1$  km and  $\lambda_h\sim 300$  km in the lower stratosphere during all seasons (Figure 11). For  $f/\widehat{\omega}$ , however, the mean values from the PANSY radar observations in the Antarctic ( $\sim 0.60$  for winter and  $\sim 0.65$  for summer) are larger than those by the MU radar ones at midlatitudes ( $\sim 0.47$  for winter and  $\sim 0.54$  for summer). This difference may reflect the GW characteristics at different latitudes, but other factors such as surrounding topography and dominant wind direction may also contribute to the parameters of GWs. It is also worth noting that Preusse et al. (2006) found a horizontal wavelength distribution, which is consistent with  $f/\widehat{\omega}$  that is about 0.55 to 0.7 for middle and high latitudes.

## 5. Summary and Concluding Remarks

We performed a statistical analysis of GWs in the Antarctic troposphere and lower stratosphere based on continuous observation data obtained over one year, from October 2015 to September 2016, using a full-system observation of the PANSY radar at Syowa Station. The frequency spectra of wind fluctuations covering a relatively wide range, from the inertial frequency ( $f$ ) to the Brunt-Väisälä frequency ( $N$ ), were obtained. The frequency power spectra of horizontal wind fluctuations ( $\omega P_u(\omega, z)$  and  $\omega P_v(\omega, z)$ ) and the zonal momentum flux spectra ( $\omega \text{Re} [U(\omega, z)W^*(\omega, z)]$ ) exhibited a clear isolated peak around  $f$  above a height of  $z=11$  km. This peak was continuously observed throughout the entire year except for August 2016. The peak was particularly remarkable and narrow in its frequency from January to March. In contrast, the frequency power spectra of vertical wind fluctuations ( $\omega P_w(\omega, z)$ ) did not have the peak around  $f$  in the lower stratosphere. Podglajen et al. (2016) estimated the intrinsic frequency spectra for potential energy, horizontal and vertical kinetic energy using 19 superpressure balloon observations over Antarctica and Austral ocean in September 2010 to January 2011. The horizontal wind part of kinetic energy spectra showed a peak close to the inertial frequency ( $f$ ), while there is no equivalent peak in their potential energy spectra and vertical wind part of kinetic energy spectra. The lack of the peak around  $f$  in  $\omega P_w(\omega, z)$  likely reflects the near horizontal air parcel motions associated with NIGWs. However, it should be noted that the frequencies of the NIGWs are not necessarily near close to  $f$ , as shown in the histogram of  $\hat{\omega}/f$  by the hodograph analysis (Figure 12). Furthermore, the frequency spectra for  $\overline{u'w'}$  has significant negative values around  $f$  in the lower stratosphere (Figure 3), suggesting that the air parcel motions involve vertical movements, and the peak around  $f$  corresponding to the NIGWs can be seen in vertical wind spectra. Thus, the absence of the peak near  $f$  in the observed  $\omega P_w(\omega, z)$  is likely explained by the dominance of larger vertical wind amplitudes that GWs with higher ground-based frequencies may have. It is also worth noting that the observational time period of campaigns analyzed in Podglajen et al. (2016), Concordiasi, was September 2010 to January 2011, which is different from the time period from January to March, when the a very clear peak close to  $f$  was observed by the PANSY radar.

The vertical profile of the percentages of the vertical group velocities of the NIGWs suggested that the sources of NIGWs exist near the surface and around the tropopause during the whole one year and in the lower stratosphere and/or above in winter. The results of the analyses focusing on the NIGW based on hodograph analysis can be explained by the conjecture that the most likely sources of NIGWs were surface topography, the tropospheric jet, and the polar night jet. The ground-based horizontal phase velocity of NIGWs with upward group velocity was approximately 0 m/s, which is consistent with the characteristics of the orographic waves generated over the Antarctic topography. This result is consistent with those of other observational studies performed in the polar region. Based on the ST radar observations at Davis Station in the Antarctic, Alexander and Murphy (2015) indicated that the interactions between strong winds along the Antarctic coastline and an ice ridgeline upwind of Davis formed orographic GWs. The majority of NIGWs propagating energy downward in the lower stratosphere ( $z=17\text{--}20$  km) in JJA had  $c_{\text{obs}}$  that were biased eastward, which strongly supports the conjecture that the most likely candidate for their source is the polar night jet, which blows strongly eastward in the winter stratosphere. It is interesting that the NIGWs in the troposphere and lower stratosphere have different sources, that is, Antarctic topography, the tropospheric jet, and the polar night jet, even though they exist in the same range of vertical wavelenghts and ground-based frequencies.

The quantitative knowledge about the parameters of NIGWs with vertical and seasonal dependence obtained in this study is useful for reducing uncertainties in the GW parameterizations implemented in most climate models. In future studies, the horizontal propagation of GWs (e.g., Song & Chun, 2008), the horizontal refraction in the background wind shear (e.g., Amemiya & Sato, 2016; Preusse et al., 2009; Sato et al., 2009), the horizontal advection by the background wind (e.g., Sato et al., 2012; Smith, 1980) and/or their intrinsic group velocities, and the intermittency of GW momentum fluxes (e.g., de la Cámara et al., 2014; Hertzog et al., 2012; Jewtoukoff et al., 2015; Plougonven et al., 2017) should be examined based on PANSY radar observations. Combining these data with numerical simulations will be useful. We also plan to determine why the GWs in the lower stratosphere over Syowa Station have a frequency of approximately 12 hr, which is close to the inertial frequency.

## Acknowledgments

All figures in this paper were created using Dennon Club Library (DCL). This work was supported by JSPS KAKENHI grants 201703536 and by JST CREST JPMJCR1663. I would like to thank Y. Tomikawa, M. Kohma, and R. Shibuya for their many valuable comments and discussions. The PANSY multi-institutional project was operated by the University of Tokyo and the National Institute of Polar Research (NIPR), and the PANSY radar system observations at Syowa Station were operated by the Japanese Antarctic Research Expedition. The PANSY radar observation data are available at the project website, <http://pansy.eps.s.u-tokyo.ac.jp>. PANSY high-resolution data used in this study are described in Sato et al. (2014) and available by request. Contact Kaoru Sato ([kaoru@eps.s.u-tokyo.ac.jp](mailto:kaoru@eps.s.u-tokyo.ac.jp)). The operational radiosonde observation data used in this study were obtained from the website of Japan Meteorological Agency (<http://www.jma.go.jp/jma/indexe.html>).

## References

- Alexander, M. J., Geller, M., McLandress, C., Polavarapu, S., Preusse, P., Sassi, F., et al. (2010). Recent developments in gravity-wave effects in climate models and the global distribution of gravity-wave momentum flux from observations and models. *Quarterly Journal of the Royal Meteorological Society*, *136*, 1103–1124. <https://doi.org/10.1002/qj.637>
- Alexander, M. J., & Grimsdell, A. W. (2013). Seasonal cycle of orographic gravity wave occurrence above small islands in the Southern Hemisphere: Implications for effects on the general circulation. *Journal of Geophysical Research: Atmospheres*, *118*, 11,589–11,599. <https://doi.org/10.1002/2013JD020526>
- Alexander, S., & Murphy, D. (2015). The seasonal cycle of lower-tropospheric gravity wave activity at Davis, Antarctica (69°S, 78°E). *Journal of the Atmospheric Sciences*, *72*(3), 1010–1021. <https://doi.org/10.1175/JAS-D-14-0171.1>
- Alexander, S. P., Klekociuk, A. R., & Tsuda, T. (2009). Gravity wave and orographic wave activity observed around the Antarctic and Arctic stratospheric vortices by the COSMIC GPS-RO satellite constellation. *Journal of Geophysical Research*, *114*, D17103. <https://doi.org/10.1029/2009JD011851>
- Alexander, S. P., Murphy, D. J., & Klekociuk, A. R. (2013). High resolution VHF radar measurements of tropopause structure and variability at Davis, Antarctica (69°S, 78°E). *Atmospheric Chemistry and Physics*, *13*(6), 3121–3132. <https://doi.org/10.5194/acp-13-3121-2013>
- Amemiya, A., & Sato, K. (2016). A new gravity wave parameterization including three-dimensional propagation. *Journal of the Meteorological Society of Japan. Ser. II*, *94*(3), 237–256. <https://doi.org/10.2151/jmsj.2016-013>
- Arnault, J., & Kirkwood, S. (2012). Dynamical influence of gravity waves generated by the Vestfjella Mountains in Antarctica: Radar observations, fine-scale modelling and kinetic energy budget analysis. *Tellus A: Dynamic Meteorology and Oceanography*, *64*(1), 17261. <https://doi.org/10.3402/tellusa.v64i0.17261>
- Becker, E. (2012). Dynamical control of the middle atmosphere. *Space Science Reviews*, *168*(1–4), 283–314. <https://doi.org/10.1007/s11214-011-9841-5>
- Birner, T., Dörnbrack, A., & Schumann, U. (2002). How sharp is the tropopause at midlatitudes? *Geophysical Research Letters*, *29*(14), 1700. <https://doi.org/10.1029/2002GL015142>
- Blackman, R. B., & Tukey, J. W. (1959). *The measurement of power spectra* (Vol. first).
- de la Cámara, A., Lott, F., & Hertzog, A. (2014). Intermittency in a stochastic parameterization of nonorographic gravity waves. *Journal of Geophysical Research: Atmospheres*, *119*, 11,905–11,919. <https://doi.org/10.1002/2014JD022002>
- Ern, M., Preusse, P., Gille, J. C., Hoppelwhite, C. L., Mlynarczyk, M. G., Russell, J. M., & Riese, M. (2011). Implications for atmospheric dynamics derived from global observations of gravity wave momentum flux in stratosphere and mesosphere. *Journal of Geophysical Research*, *116*, D19107. <https://doi.org/10.1029/2011JD015821>
- Fritts, D. C., Smith, R. B., Taylor, M. J., Doyle, J. D., Eckermann, S. D., Dörnbrack, A., et al. (2016). The Deep Propagating Gravity Wave Experiment (DEEPWAVE): An airborne and ground-based exploration of gravity wave propagation and effects from their sources throughout the lower and middle atmosphere. *Bulletin of the American Meteorological Society*, *97*(3), 425–453. <https://doi.org/10.1175/BAMS-D-14-00269.1>
- Geller, M. A., Alexander, M. J., Love, P. T., Bacmeister, J., Ern, M., Hertzog, A., et al. (2013). A comparison between gravity wave momentum fluxes in observations and climate models. *Journal of Climate*, *26*(17), 6383–6405. <https://doi.org/10.1175/JCLI-D-12-00545.1>
- Gong, J., Wu, D. L., & Eckermann, S. D. (2012). Gravity wave variances and propagation derived from AIRS radiances. *Atmospheric Chemistry and Physics*, *12*(4), 1701–1720. <https://doi.org/10.5194/acp-12-1701-2012>
- Guest, F. M., Reeder, M. J., Marks, C. J., Karoly, D. J., Guest, F. M., Reeder, M. J., et al. (2000). Inertia-gravity waves observed in the lower stratosphere over Macquarie Island. *Journal of the Atmospheric Sciences*, *57*(5), 737–752. [https://doi.org/10.1175/1520-0469\(2000\)057%3C0737:IGWOIT%3E2.0.CO;2](https://doi.org/10.1175/1520-0469(2000)057%3C0737:IGWOIT%3E2.0.CO;2)
- Hei, H., Tsuda, T., & Hirooka, T. (2008). Characteristics of atmospheric gravity wave activity in the polar regions revealed by GPS radio occultation data with CHAMP. *Journal of Geophysical Research*, *113*, D04107. <https://doi.org/10.1029/2007JD008938>
- Hertzog, A., Alexander, M. J., & Plougonven, R. (2012). On the intermittency of gravity wave momentum flux in the stratosphere. *Journal of the Atmospheric Sciences*, *69*(11), 3433–3448. <https://doi.org/10.1175/JAS-D-12-09.1>
- Hertzog, A., Boccarra, G., Vincent, R. A., Vial, F., & Cocquerez, P. (2008). Estimation of gravity wave momentum flux and phase speeds from quasi-Lagrangian stratospheric balloon flights. Part II: Results from the Vorcore campaign in Antarctica. *Journal of the Atmospheric Sciences*, *65*(10), 3056–3070. <https://doi.org/10.1175/2008JAS2710.1>
- Hertzog, A., Cocquerez, P., Guilbon, R., Valdivia, J.-N., Venel, S., Basdevant, C., et al. (2007). Stratéole/Vorcore—long-duration, superpressure balloons to study the Antarctic lower stratosphere during the 2005 winter. *Journal of Atmospheric and Oceanic Technology*, *24*(12), 2048–2061. <https://doi.org/10.1175/2007JTECHA948.1>
- Hertzog, A., Vial, F., Mechoso, C. R., Basdevant, C., & Cocquerez, P. (2002). Quasi-Lagrangian measurements in the lower stratosphere reveal an energy peak associated with near-inertial waves. *Geophysical Research Letters*, *29*(8), 1229. <https://doi.org/10.1029/2001GL014083>
- Hindley, N. P., Wright, C. J., Smith, N. D., & Mitchell, N. J. (2015). The southern stratospheric gravity wave hot spot: Individual waves and their momentum fluxes measured by COSMIC GPS-RO. *Atmospheric Chemistry and Physics*, *15*(14), 7797–7818. <https://doi.org/10.5194/acp-15-7797-2015>
- Hirota, I., & Niki, T. (1986). Inertia-gravity waves in the troposphere and stratosphere observed by the MU radar. *Journal of the Meteorological Society of Japan. Ser. II*, *64*(6), 995–999. [https://doi.org/10.2151/jmsj1965.64.6\\_995](https://doi.org/10.2151/jmsj1965.64.6_995)
- Hoffmann, L., Xue, X., & Alexander, M. J. (2013). A global view of stratospheric gravity wave hotspots located with Atmospheric Infrared Sounder observations. *Journal of Geophysical Research: Atmospheres*, *118*, 416–434. <https://doi.org/10.1029/2012JD018658>
- Jewtoukoff, V., Hertzog, A., Plougonven, R., de la Cámara, A., & Lott, F. (2015). Comparison of gravity waves in the southern hemisphere derived from balloon observations and the ECMWF analyses. *Journal of the Atmospheric Sciences*, *72*(9), 3449–3468. <https://doi.org/10.1175/JAS-D-14-0324.1>
- Lindzen, R. S. (1981). Turbulence and stress owing to gravity wave and tidal breakdown. *Journal of Geophysical Research*, *86*(C10), 9707. <https://doi.org/10.1029/JC086iC10p09707>
- Minamiyama, Y., Sato, K., Kohma, M., & Tsutsumi, M. (2016). Characteristics of vertical wind fluctuations in the lower troposphere at syowa station in the antarctic revealed by the PANSY radar. *Scientific Online Letters on the Atmosphere*, *12*(0), 116–120. <https://doi.org/10.2151/sola.2016-026>
- Moffat-Griffin, T., & Colwell, S. R. (2017). The characteristics of the lower stratospheric gravity wavefield above Halley (75°S, 26°W), Antarctica, from radiosonde observations. *Journal of Geophysical Research: Atmospheres*, *122*, 8998–9010. <https://doi.org/10.1002/2017JD027079>
- Moffat-Griffin, T., Hibbins, R. E., Jarvis, M. J., & Colwell, S. R. (2011). Seasonal variations of gravity wave activity in the lower stratosphere over an Antarctic Peninsula station. *Journal of Geophysical Research*, *116*, D14111. <https://doi.org/10.1029/2010JD015349>

- Murphy, D. J., Alexander, S. P., Klekociuk, A. R., Love, P. T., & Vincent, R. A. (2014). Radiosonde observations of gravity waves in the lower stratosphere over Davis, Antarctica. *Journal of Geophysical Research: Atmospheres*, *119*, 11,973–11,996. <https://doi.org/10.1002/2014JD022448>
- Nastrom, G. D., & Eaton, F. D. (2006). Quasi-monochromatic inertia-gravity waves in the lower stratosphere from MST radar observations. *Journal of Geophysical Research*, *111*, D19103. <https://doi.org/10.1029/2006JD007335>
- Pavelin, E., Whiteway, J. A., & Vaughan, G. (2001). Observation of gravity wave generation and breaking in the lowermost stratosphere. *Journal of Geophysical Research*, *106*(D6), 5173–5179. <https://doi.org/10.1029/2000JD900480>
- Pfenninger, M., Liu, A. Z., Papen, G. C., & Gardner, C. S. (1999). Gravity wave characteristics in the lower atmosphere at south pole. *Journal of Geophysical Research*, *104*(D6), 5963–5984. <https://doi.org/10.1029/98JD02705>
- Plougonven, R., Jewtoukoff, V., de la Cámara, A., Lott, F., & Hertzog, A. (2017). On the relation between gravity waves and wind speed in the lower stratosphere over the Southern Ocean. *Journal of the Atmospheric Sciences*, *74*(4), 1075–1093. <https://doi.org/10.1175/JAS-D-16-0096.1>
- Plougonven, R., Teitelbaum, H., & Zeitlin, V. (2003). Inertia gravity wave generation by the tropospheric midlatitude jet as given by the Fronts and Atlantic Storm-Track Experiment radio soundings. *Journal of Geophysical Research*, *108*(D21), 4686. <https://doi.org/10.1029/2003JD003535>
- Plumb, R. A. (2002). Stratospheric transport. *Journal of the Meteorological Society of Japan. Ser. II*, *80*(4B), 793–809. <https://doi.org/10.2151/jmsj.80.793>
- Podglajen, A., Hertzog, A., Plougonven, R., & Legras, B. (2016). Lagrangian temperature and vertical velocity fluctuations due to gravity waves in the lower stratosphere. *Geophysical Research Letters*, *43*, 3543–3553. <https://doi.org/10.1002/2016GL068148>
- Preusse, P., Ern, M., Eckermann, S. D., Warner, C. D., Picard, R. H., Knieling, P., et al. (2006). Tropopause to mesopause gravity waves in August: Measurement and modeling. *Journal of Atmospheric and Solar-Terrestrial Physics*, *68*(15), 1730–1751. <https://doi.org/10.1016/J.JASTP.2005.10.019>
- Preusse, P., Schroeder, S., Hoffmann, L., Ern, M., Friedl-Vallon, F., Ungermann, J., et al. (2009). New perspectives on gravity wave remote sensing by spaceborne infrared limb imaging. *Atmospheric Measurement Techniques*, *2*(1), 299–311. <https://doi.org/10.5194/amt-2-299-2009>
- Rabier, F., Bouchard, A., Brun, E., Doerenbecher, A., Guedj, S., Guidard, V., et al. (2010). The Concordiasi project in Antarctica. *Bulletin of the American Meteorological Society*, *91*(1), 69–86. <https://doi.org/10.1175/2009BAMS2764.1>
- Sato, K. (1990). Vertical wind disturbances in the troposphere and lower stratosphere observed by the MU radar. *Journal of the Atmospheric Sciences*, *47*(23), 2803–2817. [https://doi.org/10.1175/1520-0469\(1990\)047%3C2803:VWDITT%3E2.0.CO;2](https://doi.org/10.1175/1520-0469(1990)047%3C2803:VWDITT%3E2.0.CO;2)
- Sato, K. (1993). Small-scale wind disturbances observed by the MU radar during the passage of typhoon Kelly. *Journal of the Atmospheric Sciences*, *50*(4), 518–537. [https://doi.org/10.1175/1520-0469\(1993\)050%3C0518:SSWDOB%3E2.0.CO;2](https://doi.org/10.1175/1520-0469(1993)050%3C0518:SSWDOB%3E2.0.CO;2)
- Sato, K. (1994). A statistical study of the structure, saturation and sources of inertia-gravity waves in the lower stratosphere observed with the MU radar. *Journal of Atmospheric and Terrestrial Physics*, *56*(6), 755–774. [https://doi.org/10.1016/0021-9169\(94\)90131-7](https://doi.org/10.1016/0021-9169(94)90131-7)
- Sato, K., Kohma, M., Tsutsumi, M., & Sato, T. (2017). Frequency spectra and vertical profiles of wind fluctuations in the summer Antarctic mesosphere revealed by MST radar observations. *Journal of Geophysical Research: Atmospheres*, *122*, 3–19. <https://doi.org/10.1002/2016JD025834>
- Sato, K., Kumakura, T., & Takahashi, M. (1999). Gravity waves appearing in a high-resolution GCM simulation. *Journal of the Atmospheric Sciences*, *56*(8), 1005–1018. [https://doi.org/10.1175/1520-0469\(1999\)056%3C1005:GWAIH%3E2.0.CO;2](https://doi.org/10.1175/1520-0469(1999)056%3C1005:GWAIH%3E2.0.CO;2)
- Sato, K., O'Sullivan, D. J., & Dunkerton, T. J. (1997). Low-frequency inertia-gravity waves in the stratosphere revealed by three-week continuous observation with the MU radar. *Geophysical Research Letters*, *24*(14), 1739–1742. <https://doi.org/10.1029/97GL01759>
- Sato, K., Tateno, S., Watanabe, S., & Kawatani, Y. (2012). Gravity wave characteristics in the southern hemisphere revealed by a high-resolution middle-atmosphere general circulation model. *Journal of the Atmospheric Sciences*, *69*(4), 1378–1396. <https://doi.org/10.1175/JAS-D-11-0101.1>
- Sato, K., Tsutsumi, M., Sato, T., Nakamura, T., Saito, A., Tomikawa, Y., et al. (2014). Program of the Antarctic Syowa MST/IS radar (PANSY). *Journal of Atmospheric and Solar-Terrestrial Physics*, *118*, 2–15. <https://doi.org/10.1016/j.jastp.2013.08.022>
- Sato, K., Watanabe, S., Kawatani, Y., Tomikawa, Y., Miyazaki, K., & Takahashi, M. (2009). On the origins of mesospheric gravity waves. *Geophysical Research Letters*, *36*, L19801. <https://doi.org/10.1029/2009GL039908>
- Sato, K., & Yoshiki, M. (2008). Gravity wave generation around the polar vortex in the stratosphere revealed by 3-hourly radiosonde observations at Syowa Station. *Journal of the Atmospheric Sciences*, *65*(12), 3719–3735. <https://doi.org/10.1175/2008JAS2539.1>
- Shibuya, R., Sato, K., Tomikawa, Y., Tsutsumi, M., & Sato, T. (2015). A study of multiple tropopause structures caused by inertia-gravity waves in the Antarctic. *Journal of the Atmospheric Sciences*, *72*(5), 2109–2130. <https://doi.org/10.1175/JAS-D-14-0228.1>
- Smith, R. B. (1980). Linear theory of stratified hydrostatic flow past an isolated mountain. *Tellus*, *32*(4), 348–364. <https://doi.org/10.3402/tellusa.v32i4.10590>
- Smith, R. B., Nugent, A. D., Kruse, C. G., Fritts, D. C., Doyle, J. D., Eckermann, S. D., et al. (2016). Stratospheric gravity wave fluxes and scales during DEEPWAVE. *Journal of the Atmospheric Sciences*, *73*(7), 2851–2869. <https://doi.org/10.1175/JAS-D-15-0324.1>
- Song, I.-S., & Chun, H.-Y. (2008). A Lagrangian spectral parameterization of gravity wave drag induced by cumulus convection. *Journal of the Atmospheric Sciences*, *65*(4), 1204–1224. <https://doi.org/10.1175/2007JAS2369.1>
- Thomas, L., Worthington, R. M., & McDonald, A. J. (1999). Inertia-gravity waves in the troposphere and lower stratosphere associated with a jet stream exit region. *Annales Geophysicae*, *17*(1), 115–121. <https://doi.org/10.1007/s00585-999-0115-4>
- Tomikawa, Y., Nishimura, Y., & Yamanouchi, T. (2009). Characteristics of tropopause and tropopause inversion layer in the polar region. *SOLA*, *5*, 141–144. <https://doi.org/10.2151/sola.2009-036>
- Vaughan, G., & Worthington, R. M. (2007). Inertia-gravity waves observed by the UK MST radar. *Quarterly Journal of the Royal Meteorological Society*, *133*(S2), 179–188. <https://doi.org/10.1002/qj.142>
- Wang, L., & Alexander, M. J. (2010). Global estimates of gravity wave parameters from GPS radio occultation temperature data. *Journal of Geophysical Research*, *115*, D21122. <https://doi.org/10.1029/2010JD013860>
- Worthington, R. M., & Thomas, L. (1997). Impact of the tropopause on upward propagation of mountain waves. *Geophysical Research Letters*, *24*(9), 1071–1074. <https://doi.org/10.1029/97GL00833>
- Wu, D. L., & Jiang, J. H. (2002). MLS observations of atmospheric gravity waves over Antarctica. *Journal of Geophysical Research*, *107*(D24), 4773. <https://doi.org/10.1029/2002JD002390>
- Wu, D. L., Preusse, P., Eckermann, S. D., Jiang, J. H., Juarez, M. T., Coy, L., & Wang, D. Y. (2006). Remote sounding of atmospheric gravity waves with satellite limb and nadir techniques. *Advances in Space Research*, *37*(12), 2269–2277. <https://doi.org/10.1016/j.asr.2005.07.031>

- Yamashita, C., Chu, X., Liu, H.-L., Espy, P. J., Nott, G. J., & Huang, W. (2009). Stratospheric gravity wave characteristics and seasonal variations observed by lidar at the South Pole and Rothera, Antarctica. *Journal of Geophysical Research*, *114*, D12101. <https://doi.org/10.1029/2008JD011472>
- Yoshiki, M., Kizu, N., & Sato, K. (2004). Energy enhancements of gravity waves in the Antarctic lower stratosphere associated with variations in the polar vortex and tropospheric disturbances. *Journal of Geophysical Research*, *109*, D23104. <https://doi.org/10.1029/2004JD004870>
- Yoshiki, M., & Sato, K. (2000). A statistical study of gravity waves in the polar regions based on operational radiosonde data. *Journal of Geophysical Research*, *105*(D14), 17,995–18,011. <https://doi.org/10.1029/2000JD900204>
- Zink, F., & Vincent, R. A. (2001). Wavelet analysis of stratospheric gravity wave packets over Macquarie Island: 1. Wave parameters. *Journal of Geophysical Research*, *106*(D10), 10,275–10,288. <https://doi.org/10.1029/2000JD900847>
- Zülicke, C., & Peters, D. (2006). Simulation of inertia-gravity waves in a poleward-breaking Rossby wave. *Journal of the Atmospheric Sciences*, *63*(12), 3253–3276. <https://doi.org/10.1175/JAS3805.1>